Semiclassical Scattering on Conical Intersections

Andrei Piryatinski,[1,*] Misha Stepanov,[1,2] Sergei Tretiak,[1] and Vladimir Chernyak[3]

[1]*Center for Nonlinear Studies, Theoretical Division, Los Alamos National Laboratory, Los Alamos, New Mexico 87545, USA*

[2]*Institute of Automation and Electrometry, Novosibirsk 630090, Russia*

[3]*Department of Chemistry, Wayne State University, 5101 Cass Avenue, Detroit, Michigan 48202, USA*

(Received 18 November 2004; published 21 November 2005)

We apply a semiclassical approach to the scattering problem of a vibrational wave packet in the vicinity of a conical intersection of electronic energy surfaces and derive analytical expressions for the scattering matrix. The latter are valid when the scattering length that scales as $\sqrt{\hbar}$ is small and a wave packet passes through the scattering region with a constant velocity. The analytical results are in excellent agreement with numerical simulations for a realistic set of parameters.

DOI: 10.1103/PhysRevLett.95.223001 PACS numbers: 31.50.Gh, 31.15.Qg, 82.20.Kh

Nonadiabatic vibrational dynamics in the vicinity of the unavoided electronic energy surface crossing is a key to understanding many fundamental processes in photophysics and photochemistry, including radiativeless energy relaxation and photoisomerization in (bio)molecules and conformational dynamics of Jahn-Teller centers [1,2]. To address this problem, advanced theoretical methods have been developed and implemented as numerical techniques such as *ab initio* electronic structure calculations [1,3], which can be combined with semiclassical molecular dynamics (MD) [1,2,4,5]. Adiabatic semiclassical MD is usually studied using the Van Vleck propagator [6] or more advanced propagators, e.g., the Herman-Kluk [7] combined with a powerful forward-backward propagation method [8–10]. However, the analytical quantum mechanical treatment of unavoided level crossing is limited [11].

In this Letter, we develop a semiclassical approximation for the scattering problem in the vicinity of unavoided level crossing resulting in compact analytic expressions. The latter can be incorporated into large scale classical MD simulations to account for nonadiabatic surface crossing effects. We consider a molecule with N internal vibrational degrees of freedom described by a vector $\mathbf{r}$, whose two electronic energy surfaces can cross. In the vicinity of the crossing, the surfaces of interest are assumed to be well separated from the other electronic states. The full Hamiltonian then can be projected onto the subspace of the two surfaces in question [Figs. 1(a) and 1(b)]. Provided that time-reversal symmetry holds, this gives

$$\hat{\mathcal{H}} = -\sum_{j=1}^{N} \frac{\hbar^2 \nabla_j^2}{2m_j} + \mathcal{U}_0(\mathbf{r}) + \mathcal{U}_x(\mathbf{r})\hat{\sigma}_x + \mathcal{U}_z(\mathbf{r})\hat{\sigma}_z, \quad (1)$$

where $\nabla_j = \partial/\partial r_j - \hat{A}_j$ is a "long" derivative involving a vector potential $\hat{A}_j(\mathbf{r}) = \hat{\sigma}_x\hat{\sigma}_z A_j(\mathbf{r})$, and $\hat{\sigma}_x$ and $\hat{\sigma}_z$ are the Pauli matrices. The vector potential induces coupling between the adiabatic surfaces [12]. $\mathcal{U}_0$ and $\mathcal{U}_a$ ($a = x, z$) are diagonal and traceless potential energy components, respectively. In the general case of a surface crossing determined by the condition $\mathcal{U}_a(\mathbf{r}) = 0$, the intersection surface has dimension $S = N - 2$. If the rank of the matrix $\partial\mathcal{U}_a(\mathbf{r})/\partial r_j$ is 2, the crossing is *unavoided* and is referred to as a *conical intersection* (CI) [see Fig. 1(a)], in contrast to *avoided* crossing when $S = N - 1$ [1,13]. The vibrational dynamics of the Hamiltonian (1) can be exactly described by a propagator

$$\hat{G}(\mathbf{r}'', \mathbf{r}'; t) = \int_{\mathbf{x}(0)=\mathbf{r}'}^{\mathbf{x}(t)=\mathbf{r}''} \mathcal{D}\mathbf{x} \exp\left(\frac{i}{\hbar} S_0(\mathbf{x})\right)\hat{U}(\mathbf{x}), \quad (2)$$

$$\hat{U}(\mathbf{x}) = \mathsf{T}\exp\left(-\frac{i}{\hbar}\int_0^t d\tau \hat{\mathcal{U}}(\mathbf{x}(\tau)) + \int_{\mathbf{x}} dx_j \hat{A}_j\right), \quad (3)$$

where $S_0(\mathbf{x})$ is the scalar action due to the kinetic and potential, $\mathcal{U}_0(\mathbf{r})$, energies, and $\hat{\mathcal{U}}(\mathbf{r}) = \mathcal{U}_x(\mathbf{r})\hat{\sigma}_x + \mathcal{U}_z(\mathbf{r})\hat{\sigma}_z$ [see Eq. (1)]. The main problem in computing the path integral $\hat{G}$ is the evaluation of the time-ordered exponential $\hat{U}(\mathbf{x})$ [6]. We demonstrate that $\hat{U}(\mathbf{x})$ can be evaluated in the semiclassical $\hbar \to 0$ limit. This allows us to derive analytical expressions for the generalized Van Vleck propagator and an explicit form of the scattering matrix. These results give an insight into a wave packet (WP) nonadiabatic scattering while passing through the CI.

Generalizing the Van Vleck propagator to the CI, we represent the matrix elements of Eq. (2), in the semiclassical limit, as

$$G_{mn} = \frac{S_{mn}^{(s)}(\mathbf{x}_{mn})}{\sqrt{d_{mn}(\mathbf{x}_{mn})}} \exp\left(\frac{i}{\hbar} S_{mn}(\mathbf{x}_{mn})\right), \quad (4)$$

where $m, n = 1, 2$, and $\mathbf{x}_{nn}$ is the classical trajectory that goes from $\mathbf{r}'$ to $\mathbf{r}''$ on the nth adiabatic surface. S_{mn} and d_{mn} are the Van Vleck action and determinant, respectively, computed for the adiabatic dynamics [6]. The principal contribution to Eq. (4) due to scattering on the CI is

$$S_{mn}^{(s)}(\mathbf{x}_{mn}) = \exp\left(\frac{i}{\hbar}\int_{\tau_1}^{\tau_2} d\tau \mathcal{U}^{(a)}(\mathbf{x}_{mn}(\tau))\right) U_{mn}(\mathbf{x}_{mn}), \quad (5)$$

where U_{mn} is the matrix element of the time-ordered exponential [Eq. (3)], and $\mathcal{U}^{(a)}$ is the adiabatic potential on the nth (mth) adiabatic surface for $\tau < \tau_0$ ($\tau > \tau_0$). In contrast to Eq. (3), the integration in U_{mn} over τ runs from τ_1 to τ_2. The presence of the adiabatic potential

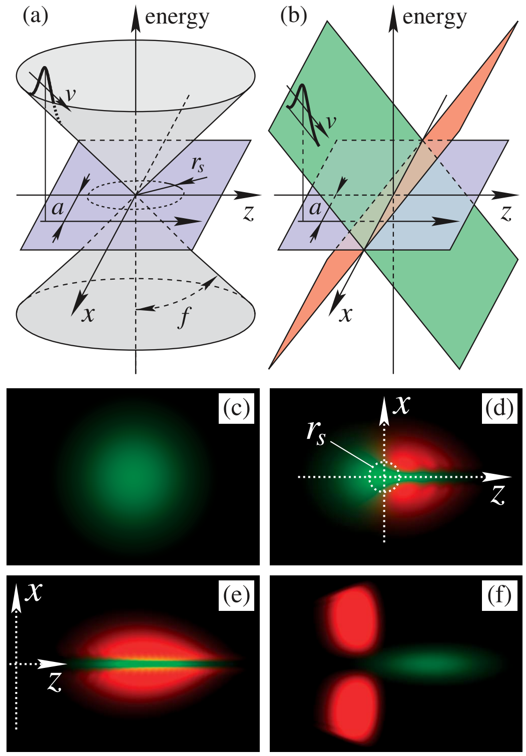

FIG. 1 (color). (a),(b) Potential energy surfaces as a function of transverse coordinates in the vicinity of the CI. A slice of the initial WP at $x = a$ with velocity v directed along the z axis is shown in (a) the adiabatic basis set and (b) the diabatic basis set (the diagonal components only), where red and green denote the $(\psi_1, 0)^T$ and $(0, \psi_2)^T$ surfaces, respectively [see Eq. (7)]. (c)–(f) Numerical simulations of the WP scattering on the CI for $g_s = 10^{-2}$ represented in the diabatic basis set. The WP is propagating in the z direction (identical in all panels). The origin of the coordinate system indicates the position of the CI. The WP component colors refer to the respective surfaces in (b), and the color brightness increases with the amplitude. The distance between the WP center and the CI center is (c) $z = -215$, (d) $z = 0$, (e) $z = 40$, and (f) $z = 300$.

$\mathcal{U}^{(a)}$ in $S_{mn}^{(s)}$ ensures cancellation of the same contribution during the time interval (τ_1, τ_2) coming from the Van Vleck action S_{mn}. Therefore, Eq. (4) defines that the pieces of the semiclassical trajectories $(\mathbf{x}(0), \mathbf{x}(\tau_1))$ and $(\mathbf{x}(\tau_2), \mathbf{x}(t))$ are described by the Van Vleck propagator, whereas the $(\mathbf{x}(\tau_1), \mathbf{x}(\tau_2))$ piece is solely propagated by the time-ordered exponential U_{mn}. Note that $S_{mn}^{(s)}$ depends weakly on the choice of the boundaries $\mathbf{x}(\tau_1)$ and $\mathbf{x}(\tau_2)$, provided they belong to the adiabatic region.

To derive the scattering matrix, we first introduce the coordinates $(x, z, \mathbf{R})$ in the vicinity of the CI [Figs. 1(a) and 1(b)], where $\mathbf{R}$ parametrizes the CI surface, whereas (x, z) are transverse coordinates orthogonal to it. In the non-adiabatic region, the vector potential components A_x and A_z, represented in the *adiabatic* basis set [Fig. 1(a)], are singular. Transformation to the *diabatic* basis [Fig. 1(b)] [12] allows one to achieve $A_x = A_z = 0$ and to represent the traceless potential as

$$\hat{\mathcal{U}}(x, z, \mathbf{R}) = (f_z(\mathbf{R})z + f_{zx}(\mathbf{R})x)\hat{\sigma}_z + f_x(\mathbf{R})x\hat{\sigma}_x. \quad (6)$$

Naturally, the diabatic basis set will be used in the scattering region throughout this Letter. In the $\hbar \to 0$ limit, the dependence of the force constants f_x, f_z, and f_{zx} on $\mathbf{R}$ can be omitted [14]. When a trajectory is far from the CI, the U_{mn} in Eq. (5) can be calculated using the adiabatic approximation. The latter breaks down in the vicinity of the CI characterized by the scattering length $r_s \propto \sqrt{\hbar}$ where, as demonstrated below, the trajectory fluctuations are weak. Therefore, we approximate the trajectory with a straight line, neglecting the WP velocity changes (ballistic approximation). Without loss of generality, we choose the z axis in the direction of the transverse velocity v. In this case, the scattering impact parameter a is measured along the x axis [see Figs. 1(a) and 1(b)].

The parameter which controls the adopted approximation can be obtained by partitioning arbitrary trajectories parametrizing $\hat{\mathcal{U}}$ [Eq. (3)] as $x(t) = a + \delta x(t)$ and $z(t) = z_1 + v(t - \tau_1) + \delta z(t)$. Here $\delta x(t)$ and $\delta z(t)$ are fluctuations with mean square values $\langle \delta x^2 \rangle \sim \langle \delta z^2 \rangle \sim \hbar(\tau_2 - \tau_1)/m$, and $m = m_x \sim m_z$. The contribution of the action accounting for the fluctuations of $\hat{\mathcal{U}}(x(t), z(t))$ to the path integral Eq. (2) scales as $f^2(\tau_2 - \tau_1)^2 \langle \delta x^2 \rangle / \hbar^2$, where $f \equiv f_z \sim f_{zx} \sim f_x$. By substituting the explicit form for $\langle \delta x^2 \rangle$ into the scaling parameter, and setting $(\tau_2 - \tau_1) = r_s/v$, the scaling parameter becomes $g_s = \sqrt{f\hbar/m^2 v^3}$. Here we have used an explicit expression for the scattering length, $r_s = \sqrt{\hbar v/f}$, justified below. We emphasize that g_s is a unique dimensionless combination of the problem parameters controlling the expansion of the fluctuating part of $\hat{U}(\mathbf{x})$ in Eq. (3). Provided $g_s \ll 1$, the effect of the fluctuations is small, and the ballistic approximation holds. Since $g_s \propto \sqrt{\hbar}$, we refer to the expansion of the full $\hat{U}(\mathbf{x})$ as the *semiclassical* one, where the time-ordered exponential in the ballistic approximation is the zero order term.

To evaluate this term, we recall that $\hat{U}(\mathbf{x})$ is a solution to the first order in a time matrix differential equation which is, in our case, precisely the Schrödinger equation. The ballistic motion of a fast ($g_s \ll 1$) WP passing through the CI is virtually unaffected by the potential. In this case, the rotation of a two-component vector $\Psi(\mathbf{r}, \tau)$ by the potential $\hat{U}(\mathbf{x})$ is the primary effect. Therefore, we can reduce the Schrödinger equation $i\hbar(\partial \mathbf{\Psi}/\partial \tau) = \hat{\mathcal{H}}\mathbf{\Psi}$ to $i\hbar(\partial \mathbf{\Psi}/\partial \tau) = \hat{\mathcal{U}}(\mathbf{r})\mathbf{\Psi}$. Here the kinetic and scalar parts of the Hamiltonian are omitted, and the position of the WP is assumed to have a straight line trajectory. Furthermore, the time τ can be replaced by $(z - z_0)/v$, and, finally, the dynamics of (z) is given by

$$i\frac{d}{dl}\Psi(l) = \frac{1}{2}(\alpha\hat{\sigma}_x + l\hat{\sigma}_z)\Psi(l), \qquad \Psi = \begin{pmatrix} \psi_1 \\ \psi_2 \end{pmatrix}, \quad (7)$$

where the dimensionless quantity $l = (\sqrt{2}/r_s)(f_{zx}a/f_z + z_0 + v\tau)$ parametrizes the trajectories, and the dimensionless impact parameter is $\alpha = \sqrt{2}f_x a/f_z r_s$. Note that they both are normalized by r_s. Equation (7) can be solved analytically on the interval (l_1, l_2) giving rise to the time-evolution operator

$$\hat{U}(l_2; l_1) = \begin{pmatrix} u_d(l_2; l_1) & u_o(l_2; l_1) \\ -\bar{u}_o(l_2; l_1) & \bar{u}_d(l_2; l_1) \end{pmatrix}, \tag{8}$$

where the diagonal and off-diagonal matrix elements are

$$u_d = \exp(-\pi\alpha^2/8)(\alpha^2 D_{\beta-1}(\eta_2) D_{\bar{\beta}-1}(\bar{\eta}_1)/4 + D_{\bar{\beta}}(\bar{\eta}_2) D_\beta(\eta_1)), \tag{9}$$

$$u_o = \alpha \exp(-\pi\alpha^2/8 + i3\pi/4)(D_{\beta-1}(\eta_2) D_{\bar{\beta}}(\bar{\eta}_1) - D_{\bar{\beta}}(\bar{\eta}_2) D_{\beta-1}(\eta_1))/2, \tag{10}$$

respectively, with $\eta = le^{-i\pi/4}$ and $\beta = i\alpha^2/4$, and the bar denotes the complex conjugate. Here $D_\nu(\eta)$ is the parabolic cylinder function [15].

Because of the weak dependence of the propagator on the boundaries l_1 and l_2, the scattering matrix $\hat{U}(\infty; -\infty)$ describing the dynamics in the vicinity of the CI is given by the leading terms in the asymptotic expansion of Eqs. (9) and (10):

$$u_d(\infty; -\infty) = \sqrt{P_d} e^{-i(\Phi_2 - \Phi_1)}, \tag{11}$$

$$u_o(\infty; -\infty) = \sqrt{P_o} e^{-i(\Phi_2 + \Phi_1) + i\delta(\alpha)}, \tag{12}$$

where $P_d = \exp(-\pi\alpha^2/2)$ ($P_o = 1 - P_d$) is the probability of a WP to stay on (to be scattered to) a diabatic surface after passing the scattering region. Note that, in the adiabatic basis set, P_d describes the scattering probability between the adiabatic surfaces [compare Figs. 1(a) and 1(b)] which resembles the Landau-Zener expression extensively used in the avoided surface crossing case [13]. The "adiabatic" phase factor $\Phi_i = (l_i^2 + \alpha^2 \ln|l_i|)/4$ depending on the initial ($i = 1$) and final ($i = 2$) trajectory points has two terms. The quadratic one causes fast oscillations of a WP, and the other, slowly varying logarithmic term, induces the impact parameter dependent shift of the oscillation period. Finally, the path independent "nonadiabatic" phase shift is $\delta(\alpha) = \pi/4 - \arg\Gamma(-i\alpha^2/4)$, where $\Gamma(z)$ is the Euler gamma function.

Equations (11) and (12) describe only forward scattering. The backscattering inducing the quantum interference of incoming and reflected WPs occurs within the scattering region r_s and is due to $O(1/l)$ terms in the asymptotic expansion of Eqs. (9) and (10). Furthermore, the probability P_d is independent of l, indicating that the WP scatters on the length scale $|l| \sim 1$, i.e., $z \sim r_s$, and P_d also decays exponentially on the length scale $a \sim r_s$. This justifies the physical meaning of r_s.

To verify the proposed approximation, we have simulated WP scattering on the CI by solving the time-dependent Schrödinger equation numerically. We set $\hbar = m = f_x = f_z = 1$ and $f_{zx} = 0$, leaving v (WP velocity) as the only parameter controlling the scattering regime, i.e., $g_s = v^{-3/2}$ and $r_s = v^{1/2}$. As illustrated in Figs. 1(a) and 1(b), the initial Gaussian WP (with the widths $\sigma = \sigma_x = \sigma_z$) is assumed to be excited to the diabatic surface above the CI, i.e., $\Psi(x, z) = (0, \psi_2)^T$ at $z = z_1 < 0$ and $|z_1| \gg r_s$. Below, scattering regimes in the range $10^{-4} \leq g_s \leq 10^{-1}$ are considered.

Figures 1(c)–1(f) shows snapshots of a WP scattering on the CI for $g = 10^{-2}$. The initial (e.g., photoexcited) WP with a broad ($\sigma = 12$) Gaussian profile [Fig. 1(c)] is launched far from the CI, where the adiabatic [Fig. 1(a)] and diabatic [Fig. 1(b)] surfaces coincide with good accuracy. The WP component ψ_2 remaining on the same diabatic surface after passing the CI becomes the scattered one from the upper to the lower adiabatic surface at z_2 [compare Figs. 1(a) and 1(b)]. In the diabatic basis set, the scattered WP [Figs. 1(d)–1(f)] should remain green after passing the CI. Figure 1(d) clearly shows that the scattering takes place within a small region of $r_s \sim 4.6$, and the fringes due to the quantum interference are resolved in the vicinity of r_s. Passing through the CI results in formation of a narrow [green strip in Fig. 1(e)] scattered WP and splitting of the remaining one into two [red blobs in Fig. 1(f)].

By propagating the WPs for different g_s, the probabilities P_d and $P_o = 1 - P_d$ can be calculated numerically as functions of the impact parameter a and compared with Eqs. (8), (11), and (12). Taking into account negligible variation of the incoming WP amplitude on the r_s, the profile of $\int dz|\psi_2(x, z)|^2$ at $z_2 \gg r_s$ should be proportional to P_d, i.e., has to be a Gaussian function of $x \equiv a$. Figure 2(a) compares numerical and analytical results for the profiles of the scattered WPs for $10^{-4} \leq g_s \leq 10^{-1}$. In the simulations, each WP approaches the scattering region with the velocity associated with g_s and the width $\sigma = 2$. Therefore, scattering probability is fully determined by the scattering radius and depends solely on the WP velocity. The graph shows that all scattered WPs are Gaussians.

To make connections with experimentally observed quantities, we have calculated quantum yield (QY) associated with the CI scattering and defined as $\int dxdz|\psi_2(x, z - z_2)|^2 / \int dxdz|\psi_2(x, z - z_1)|^2$. This quantity represents general trends in the behavior of nonradiative decay or photoisomerization rate as a function of photoexcitation energy. The inset in Fig. 2(a) compares theoretical predictions and numerical calculations of QY for the parameters adopted in Fig. 2(a). Decrease in g_s corresponds to the increase of the scattering radius and WP's photoexcitation energy. Subsequently, QY saturates for small g_s. Figure 2(a) clearly shows that the proposed approximation works extremely well for $g_s \lesssim 10^{-2}$. For $10^{-2} \leq g_s < 10^{-1}$, the theory underestimates the Gaussian WP width. As a result, theoretical QY values underestimate the numerics for 5%–10%. This discrepancy could be corrected by taking into account quantum corrections ($\sim g_s^n$, $n = 1, 2, \ldots$) to the ballistic approximation.

We next estimate g_s values for a practically interesting range of parameters. Usually, the displacements x and z are

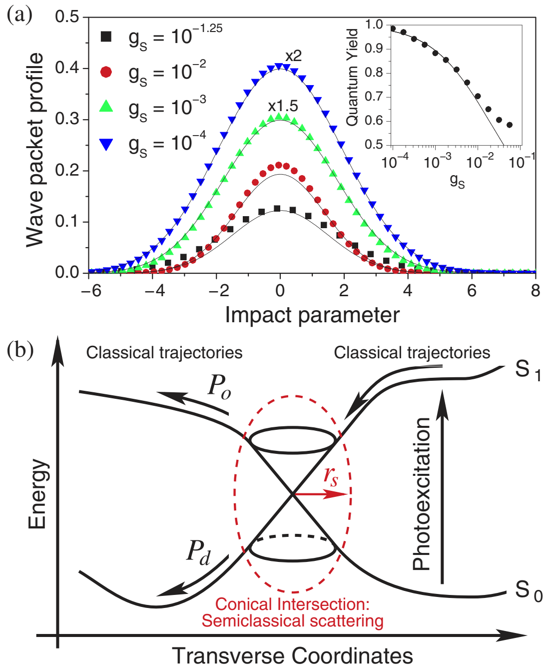

FIG. 2 (color online). (a) Asymptotic amplitude of the WPs transmitted through the CI. Points denote numerical results; solid lines represent analytical results [Eq. (11)] adjusted to the WP spreading while propagating away from the scattering region. The inset shows associated quantum yield. (b) Proposed scheme for classical large scale MD incorporating analytic treatment of nonadiabatic unavoided surface crossings.

represented by vibrational normal modes with typical energies $\nu \sim 1000\ \mathrm{cm}^{-1}$. In this case, the quantity f should be rescaled as $\kappa = \sqrt{\hbar/4\pi\nu m f} \sim 0.1$ eV (based on the data for pyrazine [1]). Then parameter g_s becomes $(h\nu\kappa^2/E_k^3)^{1/4}$, where E_k is the WP kinetic energy. If the WP is photoexcited to 0.5 eV or higher above the CI, then $g_s \lesssim 10^{-1}$ (modest estimate), and our approximation holds.

The asymptotic expressions (11) and (12) could have several practical implications for large scale MD simulations as we illustrate in Fig. 2(b). In the adiabatic regions, a classical (or semiclassical) treatment of the vibrational degrees of freedom is satisfactory. Therefore, photoexcited dynamics away from CIs can be modeled by running an ensemble of classical trajectories. If some trajectories approach the explicitly defined scattering region r_s around a CI, the dynamics becomes nonadiabatic and should be treated quantum mechanically. According to our theory, instead of numerically demanding (often intractable) quantum calculations, we propose propagating an ensemble of classical trajectories through r_s using analytic equations (8), (11), and (12) with input parameters from classical MD data. This approach is widely adopted for the case of fast passages through a simpler case of avoided crossing where the Landau-Zener theory works. Since our results are similar in spirit to the latter theory, their generalization to far more complicated cases of CIs should be efficient and universal.

In conclusion, we have derived analytical expressions for the scattering matrix in the vicinity of the CI within the semiclassical approximation, assuming that the scattering length that scales as $\sqrt{\hbar}$ is small and the ballistic approximation holds. These analytical results agree well with direct numerical simulations for $g_s \lesssim 10^{-1}$, which is consistent with a realistic range of molecular parameters. The obtained asymptotic expressions for the scattering probabilities can accelerate large scale MD simulations of (bio)-molecular clusters to account for nonadiabatic CI effects. The scattering amplitudes [Eqs. (11) and (12)] also provide a microscopic picture of the topological Berry phase [16] formation which may be detected spectroscopically. In the adiabatic (contrary to the diabatic) basis set, the scattered WP components that stay on the same adiabatic surface have different signs at positive and negative values of an impact parameter a, whereas the wave function passes zero at $a = 0$.

Work at LANL is supported by the Center for Nonlinear Studies and the LDRD program. V. C. acknowledges the support through start-up funds from Wayne State University. We thank Professor T. J. Martinez and Dr. D. Mozyrsky for stimulating discussions.

*Electronic address: apiryat@lanl.gov

[1] *Conical Intersections: Electronic Structure, Dynamics and Spectroscopy*, edited by W. Domcke, D. R. Yarkony, and H. Köppel (World Scientific, New Jersey, 2004).
[2] M. Ben-Nun, J. Quenneville, and T. J. Martinez, J. Phys. Chem. A **104**, 5161 (2000).
[3] A. Toniolo, G. Granucci, and T. J. Martinez, J. Phys. Chem. A **107**, 3822 (2003).
[4] J. C. Tully, J. Chem. Phys. **93**, 1061 (1990).
[5] M. D. Hack *et al.*, J. Chem. Phys. **115**, 1172 (2001).
[6] L. S. Schulman, *Techniques and Applications of Path Integrals* (Wiley, New York, 1981).
[7] M. F. Herman and E. Kluk, Chem. Phys. **91**, 27 (1984).
[8] X. Sun and W. H. Miller, J. Chem. Phys. **110**, 6635 (1999).
[9] K. Thompson and N. Makri, Phys. Rev. E **59**, R4729 (1999).
[10] M. Ovchinnikov, V. A. Apkarian, and G. A. Voth, J. Chem. Phys. **114**, 7130 (2001).
[11] A. Gordon and J. E. Avron, Phys. Rev. Lett. **85**, 34 (2000).
[12] M. Baer, Chem. Phys. Lett. **35**, 112 (1975).
[13] L. D. Landau and E. M. Lifshitz, *Quantum Mechanics: Non-Relativistic Theory* (Pergamon, New York, 1977).
[14] If $\hbar \rightarrow 0$, the scattering region $r_s \sim \sqrt{\hbar} \rightarrow 0$ and the wave packet motion along **R** coordinates can be neglected during the scattering event in the transverse (x, z) subspace.
[15] *Higher Transcendental Functions*, edited by A. Erdelyi (McGraw-Hill, New York, 1953), Vol. II.
[16] M. V. Berry, Proc. R. Soc. London **392**, 45 (1984).